ELSEVIER

Journal of Molecular Liquids 136 (2007) 317–322

journal of MOLECULAR LIQUIDS

www.elsevier.com/locate/molliq

Structural and dynamical characteristics of mesoscopic $H^+[H_2O]_n$ clusters

Mariano Galvagno [a], Daniel Laria [a,b], Javier Rodriguez [a,b,*]

[a] *Unidad Actividad Física, Comisión Nacional de Energía Atómica, Avenida Libertador 8250, 1429, Buenos Aires, Argentina*
[b] *Departamento de Química Inorgánica, Analítica y Química-Física e INQUIMAE, Facultad de Ciencias Exactas y Naturales, Universidad de Buenos Aires, Ciudad Universitaria, Pabellón II, 1428, Buenos Aires, Argentina*

Available online 28 August 2007

Abstract

Structural and dynamical characteristics pertaining to the solvation of an excess proton in liquid-like nanoclusters of the type $[H_2O]_n$ are investigated using Molecular Dynamics experiments. Three different aggregate sizes were analyzed: $n=10$, 21 and 125. The simulation experiments were performed using a multistate empirical valence bond Hamiltonian model. While in the smallest aggregates the proton occupies a central position, the stable solvation environments for $n=21$ and 125 are located at the cluster boundaries. In all cases, the structure of the closest solvation shell of the excess charge remains practically unchanged and coincides with that observed in bulk water. Compared to results obtained in bulk, the computed rates for proton transfer in clusters are between one and two orders of magnitude slower, and tend to increase for larger cluster sizes.

Keywords: Molecular Dynamics; Proton solvation; Water clusters

1. Introduction

The study of the solvation of ionic species in aqueous clusters is of great importance in many areas of environmental and atmospheric chemistry [1–4]. Many chemical reactions occurring in the earth atmosphere involve ions embedded at the surface of icicles. Protonated water clusters are perhaps one of the most abundant of these species in the stratosphere and can host a large variety of chemical processes; most notably are those controlling atmospheric nucleation. For example, Yang and Castleman [5] have analyzed the importance of these aggregates in the earliest stages of the formation of noctilucent clouds at high altitudes, at temperatures as low as 150 K. From a more fundamental perspective, the analysis of the equilibrium and dynamical characteristics of chemical reactivity in these clusters continues to draw considerable attention from experimental and theoretical perspectives [6]. One of the reasons for this interest is the fact that, by a careful control of the cluster sizes, one can bridge the gap between analyses of reactivity in two important limiting behaviors, *i.e.* gaseous and condensed phases.

In the present paper we examine the solvation of an excess proton in mesoscopic clusters of the type $H^+[H_2O]_n$, with sizes intermediate between $n=10$ and $n=125$. This size range covers aggregates with incipient three dimensional structures up to nanoclusters where it is possible to establish a clear distinction between inner, "bulk-like", domains and surface states. Our analysis will be based on results obtained from Molecular Dynamics simulation experiments and includes the study of the equilibrium solvation structures and dynamical aspects related to proton transfer processes as well. To tackle the problem we resorted on a multistate empirical valence bond (MS-EVB) model Hamiltonian [7–11]. This approach has been repeatedly used in the past and has proved to be sufficiently versatile so as to be successfully applied for the examination of aqueous protons in a wide variety of environments: bulk, [8–10,12–18] clusters, [19,20] confined environments, [21–23] air–water interfaces, [24] and water at extreme conditions of temperature and pressure, [25] to cite just a few important examples. The organization of the paper is as follows: in Section 2 we present a brief overview of the model and the simulation procedure. The main results are presented in Section 3. The last section contains the concluding remarks.

2. Model and simulation procedure

The systems under investigation consisted of protonated clusters of the type $H^+[H_2O]_n$, with $n=10$, 21 and 125. The

* Corresponding author.
E-mail address: jarodrig@cnea.gov.ar (J. Rodriguez).

0167-7322/$ - see front matter © 2007 Elsevier B.V. All rights reserved.
doi:10.1016/j.molliq.2007.08.008

Molecular Dynamics experiments were performed using an MS-EVB scheme. This model has been thoroughly described in previous studies, so we will present here a brief overview of its main features and refer the interested reader to Refs. [12–16], for more complete presentations. The cornerstone of the model is the following MS-EVB Hamiltonian:

$$\hat{H}_{\mathrm{EVB}}(\{\mathbf{R}\}) = \sum_{ij} |\phi_i\rangle h_{ij}(\{\mathbf{R}\})\langle\phi_j|; \tag{1}$$

where $\{|\phi_i\rangle\}$ represents a basis set of diabatic states. Each of these states denotes the spatial localization of the excess proton in a different water molecule. The matrix elements of the MS-EVB Hamiltonian, $h_{ij}(\{\mathbf{R}\})$, are parametrized in terms of the nuclear coordinates and are adjusted so that EVB predictions for the energetics and geometrical details of small protonated water clusters agree with those obtained from highly sophisticated ab initio calculations [14].

At each step of the Molecular Dynamics runs, the simulation procedure involved the construction of a connectivity pattern of hydrogen bonds (HB), linking the water molecule exhibiting strongest H_3O^+ character (hereafter referred to as the pivot water and denoted as H_2O^*) with its first, second – and eventually – third solvation shells. This pattern allowed the identification of the instantaneous diabatic states included in the construction of $\hat{H}_{\mathrm{EVB}}$. For $n=10$ and $n=20$, the number of EVB states considered was intermediate between 8 and 15; this number went up to typically 20, for simulations of the largest aggregates.

The dynamics of the classical nuclei was generated from the following Newton's equations of motions:

$$M_k \frac{\mathrm{d}^2\mathbf{R}_k}{\mathrm{d}t^2} = -\nabla_{\mathbf{R}_k}\epsilon_0(\{\mathbf{R}\}); \tag{2}$$

where $\epsilon_0(\{\mathbf{R}\})$ represents the lowest eigenvalue of the EVB Hamiltonian, namely:

$$\hat{H}_{\mathrm{EVB}}|\psi_0\rangle = \epsilon_0(\{\mathbf{R}\})|\psi_0\rangle. \tag{3}$$

In the previous equation, $|\psi_0\rangle$ is the ground state eigenstate of $\hat{H}_{\mathrm{EVB}}$, whose expression in terms of the diabatic states can be written as:

$$|\psi_0\rangle = \sum_i c_i|\phi_i\rangle. \tag{4}$$

The index of the largest expansion coefficient, c_i, identifies the instantaneous pivot water, which can be eventually updated, in the advent of a proton translocation episode.

Diagonal elements $h_{ii}(\{\mathbf{R}\})$ included inter- and intra-molecular interactions involving the H_3O^+ group and the rest of the water molecules, [14] that were modeled using the flexible TIP3 model [26]. All simulation experiments began with a ~0.5 ns preliminary thermalization stage, at temperatures close to $T\sim200$ K. In this thermal regime, the clusters exhibited structural and dynamical characteristics similar to those observed in liquid-like phases. Subsequent to this equilibration period, statistics were collected from constant energy trajectories, lasting typically ~5–10 ns.

3. Results

3.1. Solvation structures

Mesoscopic clusters represent inhomogeneous environments at the nanometer scale. Perhaps the first important question to be answered in connection with the solvation of an excess proton in a water cluster concerns the average localization of the excess charge. In this context, the consideration of two local density fields with respect to the center of mass of the cluster will be useful: The first one, $\rho_{\mathrm{CM-O}}{}^*(r)$, involves the position of the pivot water and is defined as:

$$\rho_{\mathrm{CM-O}^*}(r) = \frac{1}{4\pi r^2}\langle\delta(|\mathbf{r}_{\mathrm{O}^*} - \mathbf{R}_{\mathrm{CM}}| - r)\rangle. \tag{5}$$

Note that $\rho_{\mathrm{CM-O}}{}^*(r)$ represents the probability distribution of finding the pivot at a distance r from the center of mass of the aggregate. In the previous equation, $\mathbf{r}_{\mathrm{O}}{}^*$ and $\mathbf{R}_{\mathrm{CM}}$ denote the positions of the pivot and the center of mass of the cluster, respectively. The second density, $\rho_{\mathrm{CM-W}}(r)$, involves the rest of the water molecules and is defined as:

$$\rho_{CM-W}(r) = \frac{1}{4\pi r^2}\sum_i^{n-1}\langle\delta(|\mathbf{r}_{i=1}^{\mathrm{O}} - \mathbf{R}_{\mathrm{CM}}| - r)\rangle; \tag{6}$$

where $\mathbf{r}_i^{\mathrm{O}}$ represents the coordinate of oxygen site in the i-th molecule and the sum involves all the water molecules, except the one acting as pivot.

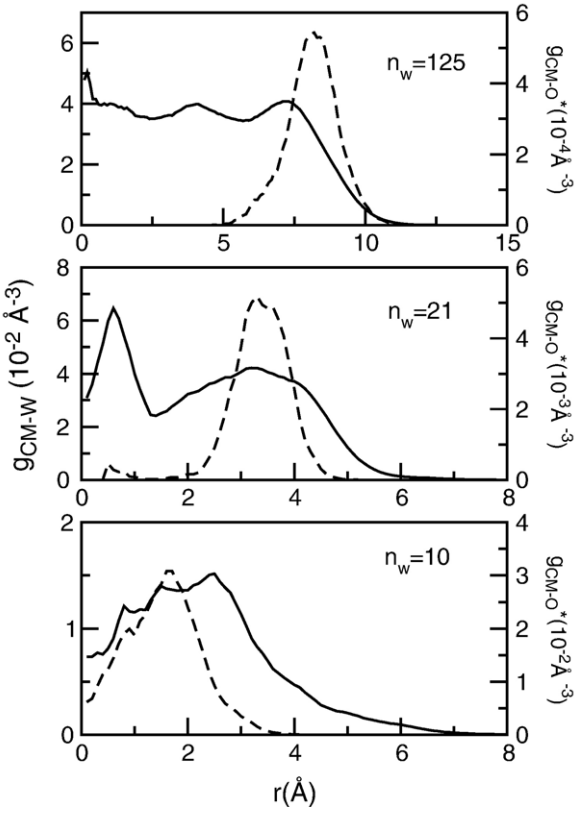

Fig. 1. Local density fields with respect to the center of mass of aqueous clusters of different sizes: water oxygen (solid line, left axis); pivot oxygen (dashed line, right axis).

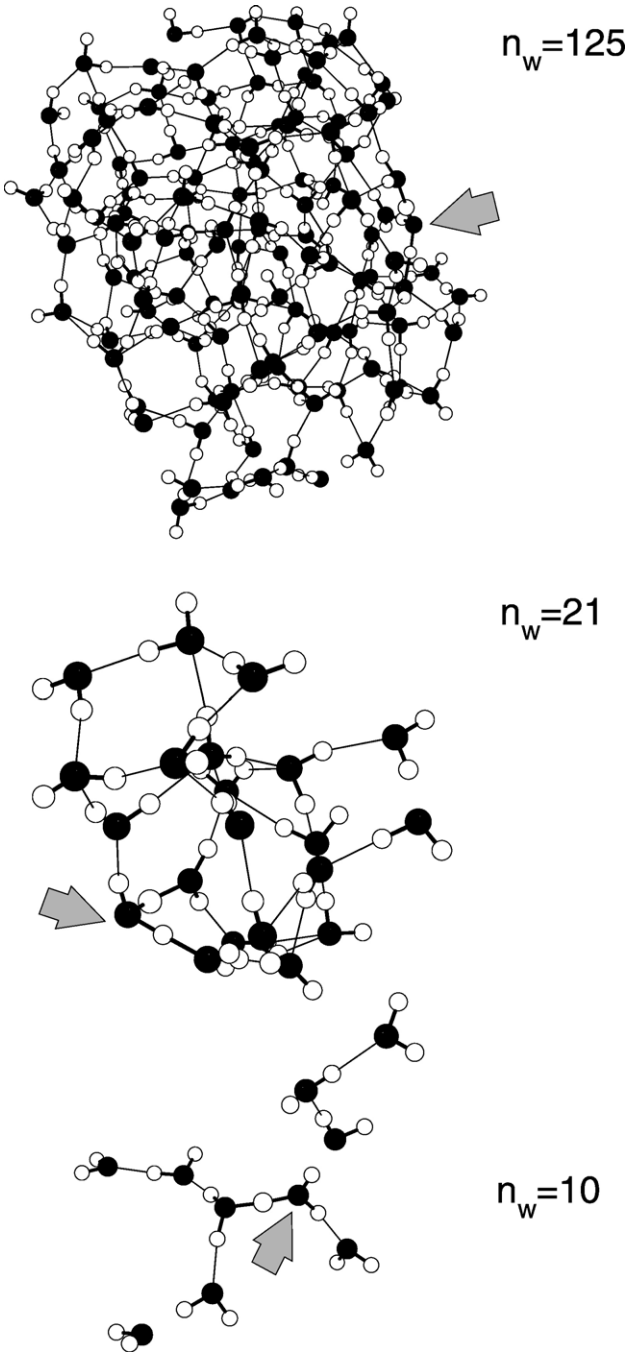

Fig. 2. Snapshots for typical configurations of protonated water clusters. The arrows indicate the instantaneous position of the pivot oxygen.

Results for both functions are depicted in Fig. 1. The profiles of the bottom panel contrast sharply to those shown in the upper ones: For the smallest size considered, $n=10$, it is evident that the excess charge localizes closer to the center of mass of the aggregate. A snapshot of a typical cluster configuration for a protonated clusters of this size is depicted in Fig. 2. Note that the overall structure looks as a mostly planar, star-like, arrangement of hydrogen bonded water molecules, with the three-coordinated hydronium lying at a central position.

The situation changes at a qualitative level in larger aggregates (see middle and top panels of Fig. 1). Under these circumstances, the water local density at the central part looks much more uniform and its value does not differ substantially from the usual one for bulk water at ambient conditions: $\rho_{CM-O}^{*}(r\sim 0)\sim\rho_{w}^{bulk}=0.033$ Å^{-3}. Snapshots for cluster configurations in this size range are also included in Fig. 2 and reveal that, in both cases, the aggregates exhibit a three-dimensional hydrogen-bonded structure, in which it is possible to discriminate bulk from surface states environments. As for the position of the proton is concerned, there are clear indications that the regions for stable proton solvation in both cases are located at the corresponding cluster boundaries. This observation has been previously reported [19] and has also been found in simulations of protons at macroscopic water–air interfaces [24].

It is also of interest to investigate the closest solvation structures of the excess charge. In bulk water, the microscopic description of such environments includes a whole series of arrangements which are intermediate between two limiting moieties, with well defined geometry: We are referring to the symmetric Zundel (ZDL) dimer [27] $[H_2O–H–OH_2]^+$ and three-coordinated Eigen (EGN) cation [28] $[H_3O\ (H_2O)_3]^+$. Interconversions between these structures take place in the picosecond time scale and seems to be triggered by changes in the intramolecular connectivity between the proton closest solvation shells. The relative prevalence of these structures can be conveniently monitored by considering probability densities associated to an appropriate order parameter identifying EGN and ZDL complexes. In the MS-EVB model, such order parameter can be expressed in terms of the two largest expansion coefficients (see Eq. (3)) as: [14,16]

$$\xi = c_1^2 - c_2^2. \tag{7}$$

ZDL and EGN solvation environments are characterized by values of ξ close to 0 and 1, respectively. In Fig. 3 we present

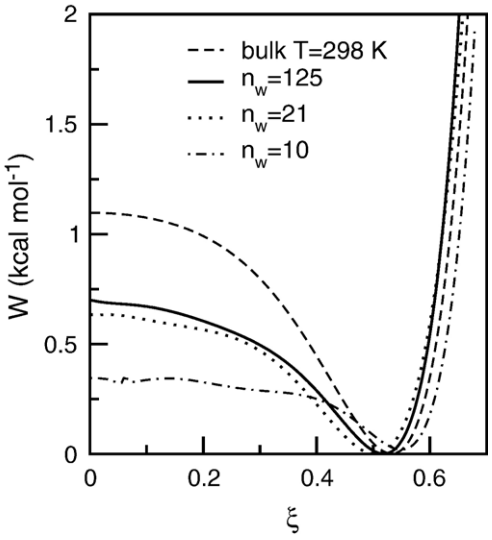

Fig. 3. Free energy associated to the asymmetric order parameter ξ describing Eigen–Zundel interconversions in protonated aqueous clusters and bulk water at ambient conditions. The curves were brought to the same reference value at their corresponding minima.

results for $W(\xi)$, the free energy associated to the order parameter:

$$\beta W(\breve{\xi}) \alpha - \ln\langle\delta(\xi - \breve{\xi})\rangle; \quad (8)$$

where β is the inverse of Boltzmann constant times the temperature and $\langle\ldots.\rangle$ represents a statistical average. For the sake of comparison, we have also included in the figure the results for bulk water reported in Refs. [14,16]. In all cases, the most stable structures – which correspond to the global minimum of $W(\xi)$ – are characterized by values of $\xi_{min} \sim 0.55$. The magnitude of the free energy differences between EGN-like and ZDL-like structures though, does depend on the particular environment considered. Results for $W(\xi=0)$ in aggregates with $n=21$ and $n=125$ are practically identical, revealing that the characteristics of the surface dynamical modes triggering EGN–ZDL interconversions are comparable for both cluster sizes. On the other hand, for $n=10$, EGN–ZDL interconversions become much more frequent and are dominated exclusively by polarization fluctuations in the aggregate. The differences in temperature preclude the direct comparison of these results to those observed in bulk water at ambient conditions; anyhow, our simulations show that the free energy barrier for the isotropic bulk phases is ~ 0.5 kcal mol^{-1} higher than the one observed at the surface of the largest clusters.

To gain additional insight on the local coordination of the excess charge, we also examined pair correlations involving the O* site. In the top panel of Fig. 4 we show plots for pair correlations between the pivot O* and oxygen (top panel) and hydrogen (bottom panel) sites in the rest of the aqueous domains. Correlations with oxygen sites are dominated by main peaks located at $r \sim 2.5$ Å which involves ~ 2.9 water–oxygen sites acting as HB acceptors. The magnitude and position of these peaks do not change with the cluster size and are similar to those observed in bulk water [14]. The overall shapes of the

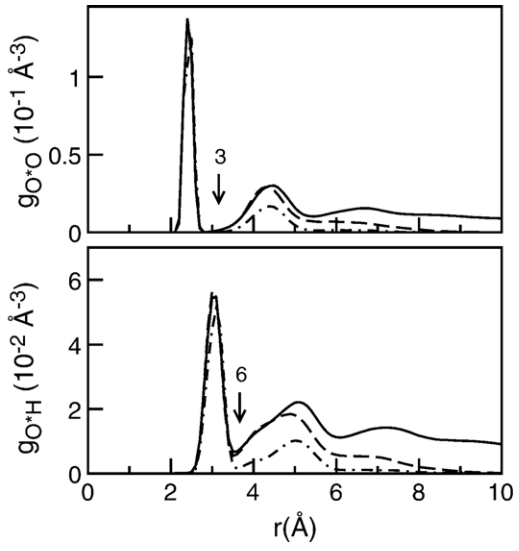

Fig. 4. Pair correlation functions between the pivot and oxygen (top panel) and hydrogen (bottom panel) sites in water clusters of different sizes. Solid line: $n=125$ (solid line); dashed line: $n=21$ dot–dashed line: $n=10$. The arrows indicate that they are under the main peaks.

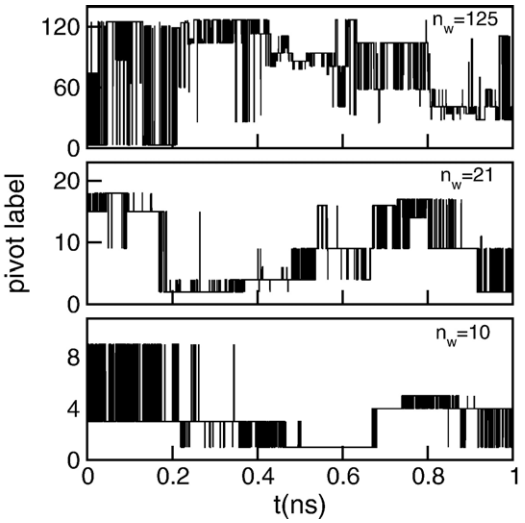

Fig. 5. Time evolutions of the pivot label in aqueous cluster of different sizes.

pivot-hydrogen profiles are also dominated by main peaks shifted ~0.6 Å outward and include six hydrogen atoms belonging to water molecules in the pivot first solvation shell. Consequently, we are led to conclude that, in all aqueous environments investigated, the closest solvation structures of the proton are preserved, being characterized by a first solvation shell composed by three water molecules, acting as HB acceptors with no evidence of pivot HB of the type O–H··· O*.

3.2. Proton transfer

Having established the main features of the equilibrium solvation structures of the proton, we now move to the

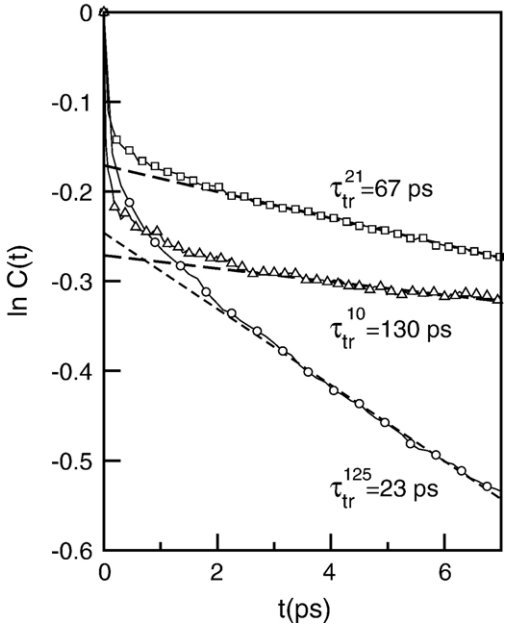

Fig. 6. Logarithm of the population relaxations for the pivot label in aqueous clusters of different sizes. $n=10$: triangles; $n=21$: squares; $n=125$: circles. The characteristic times for the transfer τ_{tr} were obtained from the inverse of the corresponding slopes at long times (dashed lines).

consideration of the dynamical characteristics related to transfer processes in aqueous clusters. In order to acquire a preliminary notion of the timescales characterizing proton translocation events in water clusters, in Fig. 5 we present the time evolutions of the pivot label during a 1 ns time interval. At a first glance, it is self-evident that proton jumps become much more frequent as we move to larger aggregates. At $T \sim 200$ K and for $n=10$, the dynamics of the pivot label can be pictured as a sequence of three well differentiated classes of episodes: (*i*) on one hand, one observes fast resonances in the subpicosecond time domain, between ZDL pairs interrupted by (*ii*) stages during which the pivot label remains practically unchanged for several hundreds of picoseconds. (*iii*) The stabilization of the proton in a different water pivot is a much more rare event since it is normally preceded by major rearrangements of the overall cluster geometry. These modifications involve changes in the localization of the potential donor and acceptor molecules, requiring the migration of the acceptor molecule towards a more central position within the aggregate. This is operated by the breakage and regeneration of new HB, that take place over lengthscales comparable to the overall size of the aggregate. Although the time evolutions of the pivot label for larger aggregates present similar qualitative characteristics, translocation episodes do occur much more frequently. Concerning possible mechanisms that might trigger transfer episodes at cluster surfaces, the direct inspection of the close vicinity of the acceptor–donor pair revealed that the transfer dynamics is operated by subtle changes in the HB structure in the second and third solvation shells. In this respect, although we have not performed a detailed trajectory analysis of reactive processes, we are led to believe that the surface mechanisms that regulate translocations resemble very much those observed in bulk macroscopic phases [30].

A more precise estimate for the proton transfer rates can be extracted from population relaxation time correlation functions of the type:

$$C(t) = \frac{\langle \delta h_i(t) \cdot \delta h_i(0) \rangle}{\langle (\delta h_i)^2 \rangle}; \qquad (9)$$

where $\delta h_i(t) = h_i(t) - \langle h_i \rangle$ denotes the instantaneous fluctuation of the population of the *i*-th reactant away from its equilibrium value. In Eq. (9), the dynamical variable $h_i(t)$ is unity if the proton is localized in the *i*-th diabatic state at time *t* and zero otherwise. Provided Onsager's regression hypothesis [29] remains valid, the exponential decay at long times of $C(t)$ should yield an estimate of the proton transfer rate, τ_{tr}^{-1}. Plots for ln $C(t)$ are presented in Fig. 6; after fast transients ascribed to ZDL resonances, the three curves present single exponential decays. Compared to the bulk result $\tau_{tr}^{blk} \sim 2$–4 ps, the estimates for the characteristic timescales in clusters are intermediate between one and two orders of magnitude larger: $\tau_{tr}^{125} \sim 20$ ps and $\tau_{tr}^{10} \sim 130$ ps.

4. Concluding remarks

The structural and dynamical characteristics of excess protons embedded in liquid-state nanoclusters of the type $H^+[H_2O]_n$ described in this paper illustrate distinctive behaviors, depending on the cluster size considered. More specifically, we focussed attention to $n=10$, 21 and 125. Taking into consideration that the cluster radii scale as $R \propto n^{1/3}$, we tried to cover different scenarios: On one hand, we considered $n \lesssim 20$ aggregates, in which it is impossible to discern surface from bulk states; on the other, $n \sim 100$ clusters – with R of the order of three molecular diameters – perhaps the smallest ones in which such distinction can be clearly established.

In small aggregates, the overall structures of $H^+[H_2O]_{10}$ clusters can be pictured as dendritic-like arrays of hydrogen bonded water molecules, with the excess proton occupying a central position. At larger sizes, there is a clear tendency for surface solvation of the excess charge. Note at in all cases, these two solvation structures preserve two important characteristics of the closest aqueous environments of the excess charge: (*i*) the three-coordinated, HB donor structure of hydronium with respect to its first solvation shell and (*ii*) the absence of HB acceptor structure of the type O–H...O*. We remark that this anisotropies have also been reported in previous cluster studies, [19,20] at water–air interfaces, [24] and confined water within membranes [22].

The observed proton dynamics in small clusters can be pictured as a sequence of three different episodes: (*i*) First, one observes resonance stages, during which the proton seems to be delocalized over a tagged ZDL pair. These fast dynamical modes of the pivot label seem to be dictated by polarization fluctuations originated in the closest solvation environments of the excess charge; (*ii*) The latter fluctuations seem to be also the controlling agent for the localization stages, during which the resonances cease and the proton gets localized in a single water molecule, for periods that may last typically ~ 100 ps; (*iii*) Finally, one also observes much rare proton translocation episodes, which are preceded by global rearrangements of the hydrogen bond connectivity of the cluster. These dynamical characteristics are maintained at a qualitative level for $n=21$ and $n=125$ aggregates, although the translocations become much more frequent and the triggering mechanisms require much more subtle modifications in the HB connectivity than those observed in smaller aggregates.

Acknowledgements

DL and JR are staff members of CONICET—Argentina.

References

[1] P. Kebarle, Annu. Rev. Phys. Chem. 28 (1997) 445.
[2] A.W. Castleman Jr., R.G. Keese, Chem. Rev. 86 (1986) 589.
[3] A.W. Castleman Jr., R.G. Keese, Annu. Rev. Phys. Chem. 37 (1986) 525.
[4] A.W. Castleman Jr., R.G. Keese, Science 241 (1988) 36.
[5] X. Yang, A.W. Castleman Jr., Geophys. Res. 96 (1991) 2573.
[6] For a recent review article on experimental and theoretical advances in the analysis of protonated aqueous clusters, see: H. Chang, C. Wu, J. Kuo, Int. Rev. Phys. Chem. 24 (2005) 553.
[7] A. Warshel, in: J. Aqvist, A. Warshel (Eds.), Computer Modeling of Chemical Reactions in Enzymes and Solutions, Chem. Rev., vol. 93, Wiley, New York, 1993, p. 2523.
[8] R. Vuilleumier, D. Borgis, J. Phys. B 102 (1998) 4261.

[9] R. Vuilleumier, D. Borgis, J. Chem. Phys. 111 (1999) 4251.
[10] D.E. Sagnella, M.E. Tuckerman, J. Chem. Phys. 108 (1998) 2073.
[11] For recent applications of MS-EVB schemes for protons in aqueous and biomolecular systems, see G. A. Voth, Acc. Chem. Res. 39 (2006)143 and references therein.
[12] J. Lobaugh, G.A. Voth, J. Chem. Phys. 104 (1996) 2056.
[13] U.W. Schmitt, G.A. Voth, J. Phys. Chem., B 102 (1998) 5547.
[14] U.W. Schmitt, G.A. Voth, J. Chem. Phys. 111 (1999) 9361.
[15] T.J.F. Day, U.W. Schmitt, G.A. Voth, J. Am. Chem. Soc. 122 (2000) 12027.
[16] T.J.F. Day, A.V. Soudackov, M. Cuma, U.W. Schmitt, G.A. Voth, J. Chem. Phys. 117 (2002) 5839.
[17] A.A. Kornyshev, A.M. Kuznetsov, E. Spohr, J. Ulstrup, J. Phys. Chem., B 107 (2003) 3351.
[18] S. Walbran, A.A. Kornyshev, J. Chem. Phys. 114 (2001) 10039.
[19] S.S. Iyengar, T.J.D. Day, G.A. Voth, Int. J. Mass Spectrom. 241 (2005) 197.
[20] S.S. Iyengar, M.K. Petersen, J.F. Day, C.J. Burnham, V.E. Teige, G.A. Voth, J. Chem. Phys. 123 (2005) 084309;
C.J. Burnham, M.K. Peterser, J.F. Dany, S.S. Iyengar, G.A. Voth, J. Chem. Phys. 124 (2006) 024327.
[21] E. Spohr, P. Commer, A.A. Kornyshev, J. Phys. Chem., B 106 (2002) 10560.
[22] M.K. Petersen, F. Wang, N.P. Blake, H. Metiu, G.A. Voth, J. Phys. Chem., B 109 (2005) 3727;
M.K. Petersen, G.A. Voth, J. Phys. Chem., B 110 (2006) 18594.
[23] H.L. Tepper, G.A. Voth, J. Phys. Chem., B 110 (2006) 21327.
[24] M.K. Petersen, S.I. Srinivasan, T.J.F. Day, G.A. Voth, J. Phys. Chem., B 108 (2004) 14804.
[25] D. Laria, J. Martí, E. Guàrdia, J. Am. Chem. Soc. 126 (2004) 2125.
[26] L.X. Dang, B.M. Pettit, J. Chem. Phys. 91 (1987) 3349.
[27] G. Zundel, H. Metzger, Z. Phys. Chem. 244 (1968) 456.
[28] M. Eigen, L. de Maeyer, Proc. R. Soc. Lond. A247 (1958) 505.
[29] D. Chandler, Introduction to Modern Statistical Mechanics (Chap. 8), Oxford University Press, New York, 1987.
[30] See for example, L. Hadas, N. Agmon, M.K. Pettersen, M.K., G. A. Voth, J. Chem. Phys. 122 (2005) 14506 and references therein.